doi:10.1016/j.jmb.2004.10.020 J. Mol. Biol. (2005) 345, 21–28

JMB

Available online at www.sciencedirect.com

SCIENCE DIRECT®

ELSEVIER

COMMUNICATION

Structural Characterization of the Ser324Thr Variant of the Catalase-peroxidase (KatG) from *Burkholderia pseudomallei*

Taweewat Deemagarn[1], Xavier Carpena[1], Rahul Singh[1], Ben Wiseman[1] Ignacio Fita[2] and Peter C. Loewen[1]*

[1]*Department of Microbiology University of Manitoba Winnipeg, MB, Canada R3T 2N2*

[2]*Consejo Superior de Investigaciones Científicas Parc Cientific, Josep Samitier 1-5 08028 Barcelona, Spain*

**Corresponding author*

The Ser315Thr variant of the catalase-peroxidase KatG from *Mycobacterium tuberculosis* imparts resistance to the pro-drug isonicotinic acid hydrazide (isoniazid) through a failure to convert it to the active drug, isonicotinoyl-NAD. The equivalent variant in KatG from *Burkholderia pseudomallei*, Ser324Thr, has been constructed, revealing catalase and peroxidase activities that are similar to those of the native enzyme. The other activities of the variant protein, including the NADH oxidase, the isoniazid hydrazinolysis and isonicotinoyl-NAD synthase activities are reduced by 60–70%. The crystal structure of the variant differs from that of the native enzyme in having the methyl group of Thr324 situated in the entrance channel to the heme cavity, in a modified water matrix in the entrance channel and heme cavity, in lacking the putative perhydroxy modification on the heme, in the multiple locations of a few side-chains, and in the presence of an apparent perhydroxy modification on the indole nitrogen atom of the active-site Trp111. The position of the methyl group of Thr324 creates a constriction or narrowing of the channel leading to the heme cavity, providing an explanation for the lower reactivity towards isoniazid and the slower rate of isonicotinoyl-NAD synthesis.

Keywords: catalase-peroxidase; isonicotinoyl-NAD; crystal structure; isoniazid

The primary role of catalase-peroxidases is the degradation of hydrogen peroxide in either a catalase:

$$2H_2O_2 \rightarrow 2H_2O + O_2$$

or a peroxidase:

$$2AH_{red} + H_2O_2 \rightarrow 2H_2O + 2A_{ox}$$

reaction, thereby preventing potential damage to cellular components by H_2O_2 and its degradation products.[1] The peroxidase reaction may have physiological significance in the production of specific products, but this remains uncertain because the *in vivo* substrate (AH_{red}) has not been identified. A low level of NADH oxidase activity has been associated recently with KatGs, but its metabolic significance is unclear.[2] The role for which KatG is most widely recognized is its involvement in the activation of the anti-tubercular pro-drug isonicotinic acid hydrazide (isoniazid or INH)[3] through its conversion to isonicotinoyl-NAD,[4–6] a competitive inhibitor of NADH in InhA, an enoyl-acyl carrier protein reductase,[4] and in KasA, a β-ketoacyl ACP synthase.[7] The result is reduced mycolic acid synthesis, which interferes with cell wall synthesis and prevents the growth of *Mycobacterium tuberculosis*. Resistance to INH is frequently associated with mutations in *katG*,[3,8] and biochemical studies have demonstrated a role for KatG in the hydrazinolysis of INH[9,10] and in the formation of isonicotinoyl-NAD.[2,5,6,11,12] Unexpectedly, these two reactions and the NADH oxidase reaction are quite distinct from the catalase and peroxidase reactions, in not requiring H_2O_2, not

Abbreviations used: INH, isonicotinic acid hydrazide or isoniazid; ABTS, 2,2′-azinobis(3-ethylbenzothiazolinesulfonic acid).

E-mail address of the corresponding author: peter_loewen@umanitoba.ca

involving heme oxidation and occurring optimally above pH 8.[2]

An understanding of the role of KatG in the formation of isonicotinoyl-NAD has not been advanced greatly by the four KatG structures reported so far: HmKatG from *Haloarcula marismortui*,[13,14], BpKatG from *Burkholderia pseudomallei*,[15,16] SyKatG from *Synechococcus* sp.[17] and recently MtKatG from *M. tuberculosis*.[18] One paramount question that remains unanswered is the location of the INH and NADH/NAD^+ binding sites in KatG, although the location of INH binding in the structurally related horse-radish peroxidase suggests a site close to the δ-meso (C_{20}) edge of the heme.[19] The Ser315Thr mutation is one of the commonest causes of INH resistance[8] and, while retaining significant catalase and peroxidase activities, the variant enzyme exhibits a reduced affinity for INH.[20] The Ser315Asn variant of MtKatG exhibits similar catalase and peroxidase activities, but with much reduced INH hydrazinolysis and isonicotinoyl-NAD synthase activities.[12]

Because BpKatG exhibits catalytic properties very similar to those of MtKatG and is amenable to crystallization, the properties of the BpKatG Ser324Thr variant, the equivalent of MtKatG Ser315Thr, were investigated, revealing catalase and peroxidase-specific activities similar to the native enzyme with only subtle differences among the kinetic parameters (Table 1). Spectral changes resulting from treatment with H_2O_2 or peracetic acid were indistinguishable (data not shown). These data suggest that the mutation has little or no effect on H_2O_2 access to the heme active site or on the binding of 2,2′-azinobis(3-ethylbenzothiazoline-sulfonic acid) (ABTS) and *o*-dianisidine, the peroxidase substrates. By contrast, both NADH oxidase and INH hydrazinolysis activities are reduced in the Ser324Thr variant compared to the native enzyme (Table 1), and this is mirrored in a slower rate of isonicotinoyl-NAD adduct formation (Figure 1). For comparison, the rate of isonicotinoyl-NAD synthesis by MtKatG is 0.41 nmol min^{-1} mg^{-1}, about 30% higher than that of BpKatG. Despite the slower reaction by the variant, the same product distribution was evident from both the variant and native enzymes after a prolonged incubation and HPLC fractionation on a reverse phase resin (data not shown).

The variant crystallized under the same conditions as the native enzyme,[15,16] and the crystals diffracted to 1.9 Å resolution (Table 2). The electron density maps defined main-chain and side-chain atoms of 1426 amino acid residues, two metal ions, two heme groups and 1733 water molecules in two subunits. As in the native enzyme, the 34

Table 1. Specific activity and kinetic constants of BpKatG and its Ser324Thr variant

	Ser324Thr	BpKatG
Catalase[a]		
Units/mg	4120±30	3,780±130
V_{max} (μmol min^{-1} μmol $heme^{-1}$)	526±27×10^3	556±14×10^3
K_m (μM)	9090±200	5,900±100
k_{cat} (s^{-1})	8770±450	9,270±230
k_{cat}/K_m (M^{-1} s^{-1})	0.96×10^6	1.6×10^6
Peroxidase[b]		
Units/mg	7.2±0.3	7.7±0.5
V_{max} (μmol min^{-1} μmol $heme^{-1}$)	830±10	1,250±30
K_m (μM)	100±5	180±5
k_{cat} (s^{-1})	13.9±0.2	20.8±0.5
k_{cat}/K_m (M^{-1} s^{-1})	1.4×10^5	1.2×10^5
NADH oxidase[c]		
Units/mg	2.0±0.1	6.9±1.0
V_{max} (μmol min^{-1} μmol $heme^{-1}$)	320±21×10^{-3}	540±96×10^{-3}
K_m (μM)	20.2±2.0	12.5±2.0
k_{cat} (s^{-1})	5.3±0.4×10^{-3}	9.0±0.4×10^{-3}
k_{cat}/K_m (M^{-1} s^{-1})	2.6×10^2	7.2×10^2
INH hydrazinolysis[d]		
Units/mg	0.38±0.05	0.93±0.02
IN-NAD synthase[e]		
Units/mg	0.08±0.004	0.29±0.04

[a] Catalase activity was determined by the method of Rørth & Jensen in a Gilson oxygraph equipped with a Clark electrode.[27] One unit of catalase is defined as the amount that decomposes 1 μmol of H_2O_2 in one minute in 60 mM H_2O_2 at pH 7.0 at 37 °C.

[b] Peroxidase activity was determined spectrophotometrically using ABTS.[28] One unit of peroxidase is defined as the amount that decomposes 1 μmol of ABTS in one minute in 0.3 mM ABTS (ε=36,800 M^{-1} cm^{-1}) and 2.5 mM H_2O_2 at pH 6.0 and 25 °C. The peroxidatic substrate *o*-dianisidine yielded similar results but the data are not reported.

[c] NADH oxidase activity was determined spectrophotometrically at 340 nm using ε=6300 M^{-1} cm^{-1} for NADH. One unit of NADH oxidase is defined as the amount that decomposes 1 nmol of NADH in a solution of 250 μM NADH at 25 °C at pH 8.75.

[d] Free radical production was assayed by NBT (nitroblue tetrazolium) reduction to a monoformazan (ε=15,000 M^{-1} cm^{-1}). One unit of INH hydrazinolysis is defined as the amount that produces 1 nmol of radical in a solution of 25 μM INH at 25 °C and pH 8.0. Protein was estimated according to the methods outlined by Layne.[29]

[e] One unit of IN-NAD synthase is defined as the amount that produces 1 nmol of IN-NAD in a solution described in the legend to Figure 1 in one minute.

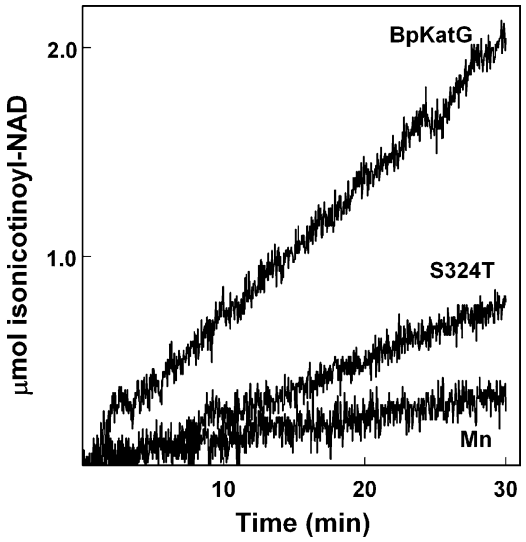

Figure 1. Rate of synthesis of the isonicotinoyl-NAD adduct. The reaction mixture contained 100 μM NAD^+, 200 μM INH, 2 μM $MnCl_2$, in 50 mM Tris–HCl (pH 8.0). No protein was added to the control labeled Mn and 200 μg of either native BpKatG or its Ser324Thr variant was added as indicated. Absorbance at 326 nm was monitored and an extinction coefficient[23] of 6900 $M^{-1}\,cm^{-1}$ was used to calculate the amount of isonicotinoyl-NAD formed, assuming no interference from other minor products formed in the reaction.[2]

Table 2. Data collection and structural refinement statistics for the Ser324Thr variant of KatG from *B. pseudomallei*

Data collection statistics	
Space group	$P2_12_12_1$
Unit cell parameters	
a(Å)	100.5
b (Å)	114.6
c(Å)	174.9
α, β, γ (deg.)	90 90 90
Resolution (Å)	30–1.9 (1.94–1.90)[a]
Unique reflections	157,135 (10,390)
Completeness (%)	99.4 (100.0)
R_{sym}[b]	0.079 (0.62)
$\langle I/\sigma I\rangle$ (%)	10.5
Multiplicity	3.7
Model refinement statistics	
No. reflections	149,065
R_{cryst}[c] (%)	17.5
R_{free}[d] (%)	21.5
Non-hydrogen atoms	11,289
Water molecules	1733
Average *B*-factor (Å^2)	
Protein	23.19
Prosthetic group	16.19
Sodium ions	20.73
Water	34.09
rms deviations	
Bond lengths (Å)	0.011
Bond angles (deg.)	1.244

The S324T variant of BpKatG was expressed from a plasmid constructed[30] and purified from the catalase-deficient *E. coli* strain UM262.[15] Crystals were obtained at 20 °C by the vapor-diffusion, hanging-drop method with 2 μl of a 22 mg/ml protein solution and 1 μl of the reservoir solution containing 16–20% (w/v) PEG 4K, 20% (v/v) methyl-2,4-pentanediol (MPD) and 0.1 M sodium citrate (pH 5.6) prepared from trisodium citrate and HCl.[15] Diffraction data were obtained from crystals cooled with a nitrogen cryo-stream using the same reservoir solution as cryobuffer at 20% PEG-4K. Crystals were primitive orthorhombic space group $P2_12_12_1$ with one dimeric molecule in the crystal asymmetric unit. The diffraction data set was processed using the program DENZO and scaled with the program SCALEPACK:[31] 5% of the measured reflections in every data set were reserved for R_{free} monitoring during automatic refinement (Table 1). Structure determination was carried out with the program AMoRe[32] and BpKatG as searching model. Refinement was carried out using REFMAC[33] with solvent molecules modeled with the program WATPEAK[34] and manually with the graphics program O.[35]

[a] Values in parentheses correspond to the highest-resolution shell.

[b] $R_{sym} = \sum_{hkl}\sum_j |I_{hkl,j} - \langle I_{hkl}\rangle| / \sum_{hkl}\langle I_{hkl}\rangle$, where *j* extends to all the observed *hkl* symmetry-related reflections.

[c] $R_{cryst} = \sum||F_{obs}| - |F_{calc}|| / \sum|F_{obs}|$.

[d] R_{free} is as for R_{cryst} but calculated for a test set, comprising 5% of reflections, that was not used in the refinement.

N-terminal residues are not visible, but the maps show clear continuity from Asn35 to Ala748 in two subunits. A number of significant differences when compared to the structure of native BpKatG are evident in the vicinity of the mutated Thr324 in the channel leading to the heme, in the distal heme pocket itself and in the double conformations of several residues.

Electron density corresponding to the methyl group of the Thr324 is clearly evident (Figure 2(a)) and persists in the $F_o - F_c$ electron density maps calculated with Ser in the model. There is a small change in conformation of the main-chain atoms including a small displacement of the adjacent main-chain carbonyl oxygen atoms (Figure 2(b)). While these appear to be very subtle changes, their effect on isonicotinoyl-NAD synthesis and INH affinity is significant.[20] The INH binding site in KatG has not been identified, but a possible site has been proposed, based on the INH binding site on horse-radish peroxidase, in a cavity on the distal side of the heme close to its δ-meso edge.[19] To reach this cavity, INH would have to pass through the channel leading to the heme cavity, passing adjacent to Ser324. A calculated surface diagram reveals the channel in the native enzyme adjacent to residue 324 (Figure 3(a)) to be significantly wider than the channel in the Ser324Thr variant (Figure 3(b)) to the extent that a number of water molecules present in the native enzyme are absent from the variant. Consequently, it is interference with INH accessibility to the heme cavity that best explains the reduced affinity and reactivity of KatG towards INH, although the possibility of INH binding in the channel cannot be excluded, in which case the methyl group would interfere with INH binding. Other mutations of this serine residue might cause a similar blockage of the channel, but the situation may be more complex because the hydrogen bond between the hydroxyl group of Ser (and Thr) and the propionate carbonyl group would disappear. The effect that this would have on the structural integrity of the enzyme, particularly in the channel region, and the electronic environment of the heme

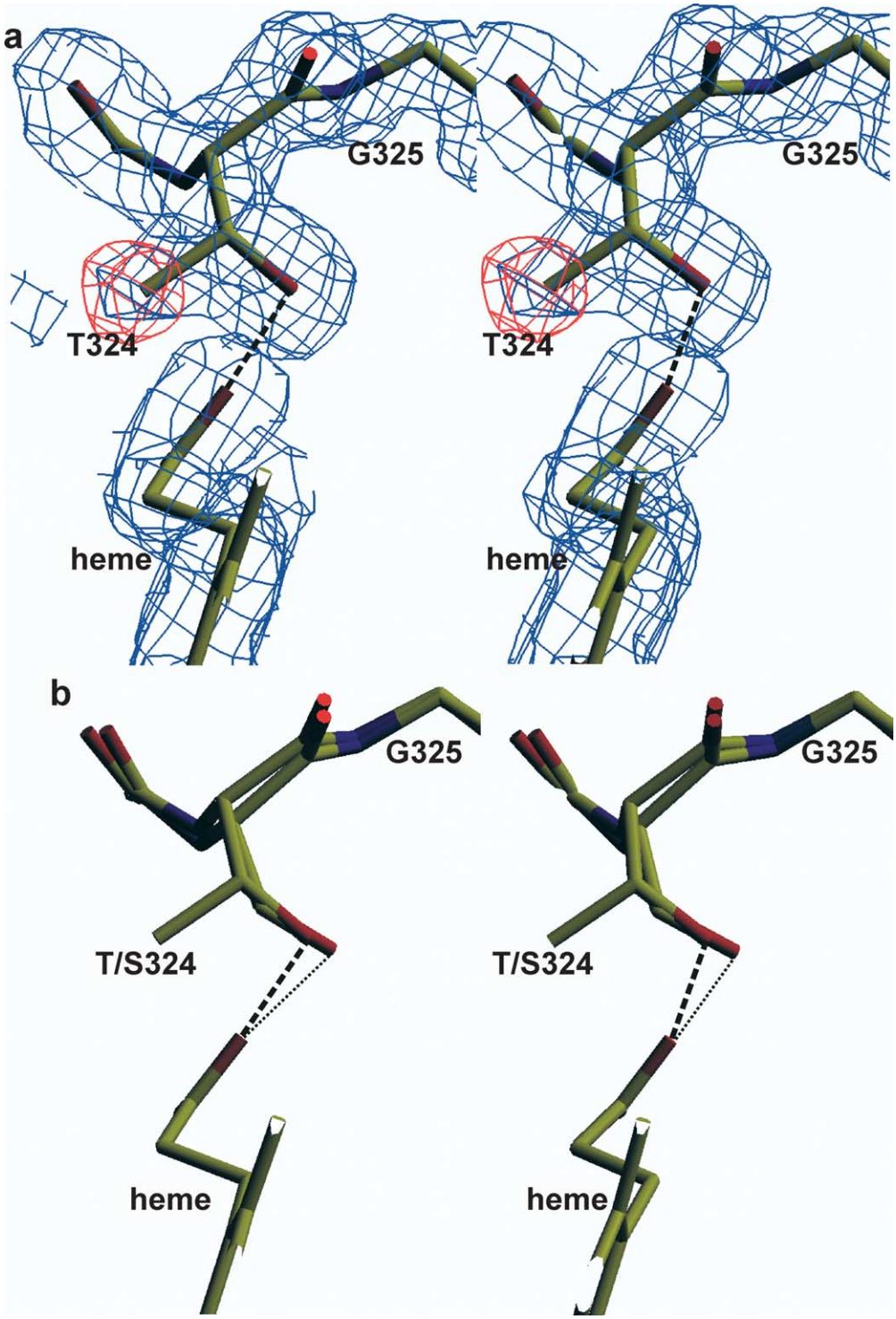

Figure 2. (a) Stereo view of the $2F_o-F_c$ (blue) electron density map of the region around Thr324 modeled at $\sigma=1.0$. The F_o-F_c (red) electron density map (modeled at $\sigma=3.0$) calculated with Ser324 in the model is superimposed. One propionate group of the heme is shown. (b) The same view of the native BpKatG model superimposed on the Ser324Thr model to illustrate the changes between the two. The hydrogen bond between the γ-OH of Thr324 and the heme propionate group is shown as a broken line. The hydrogen bond between the γ-OH of Ser324 is shown as a dotted line. The Figure was prepared using SETOR.[24]

is not clear. For example, the complete lack of isonicotinoyl-NAD synthase activity and INH hydrazinolysis activity in the Ser315Asn variant of MtKatG[12] may be the result of the larger side-chain situated in the channel or of some other distortion in the subunit arising from the lack of interaction with the heme propionate group.

Electron density suggestive of a perhydroxy

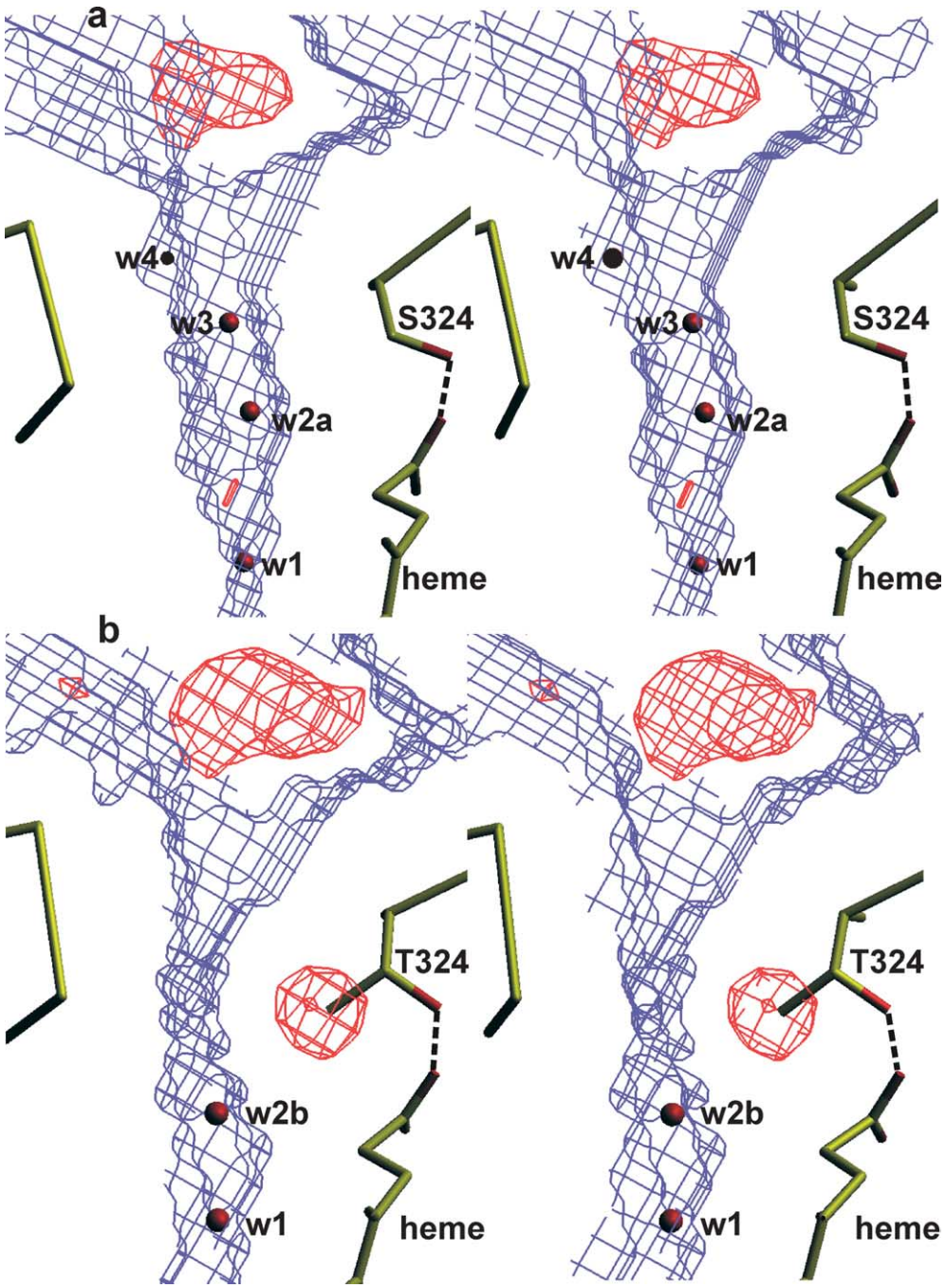

Figure 3. Stereo views of the surface maps of the channel leading to the distal heme cavity in (a) the native BpKatG and (b) the Ser324Thr variant. The narrowing of the channel in the vicinity of Thr324 is evident. The F_o-F_c (red) electron density maps (modeled at $\sigma=3.0$) calculated with Ser324 in the models are superimposed. The position of water molecules are indicated by red spheres. The hydrogen bond between the OH of Thr324 and the heme propionate group is shown as a broken line. The analysis of solvent accessibility and molecular cavities was carried out with the program VOIDOO[25] using a reduced atomic radius for polar atoms in accounting for possible hydrogen bonds.[26] The Figure was prepared using SETOR.[24]

modification on the heme in the native structure is not evident in the variant, but appears to be replaced with a similar modification on the indole nitrogen atom of Trp111 (Figure 4). The electron density maps are best explained by the second oxygen atom (hydroxy portion) of the perhydroxy group occupying two locations (A and B in Figure 4), both of which can participate in a hydrogen bond matrix involving adjacent water molecules, active-site residue side-chains and even the heme iron. The $2F_o-F_c$ map calculated assuming 50% occupancy at each of positions A and B accounts well for the available electron density, and the F_o-F_c map calculated without the modification and adjacent water molecules in the model correlates well with the putative structure

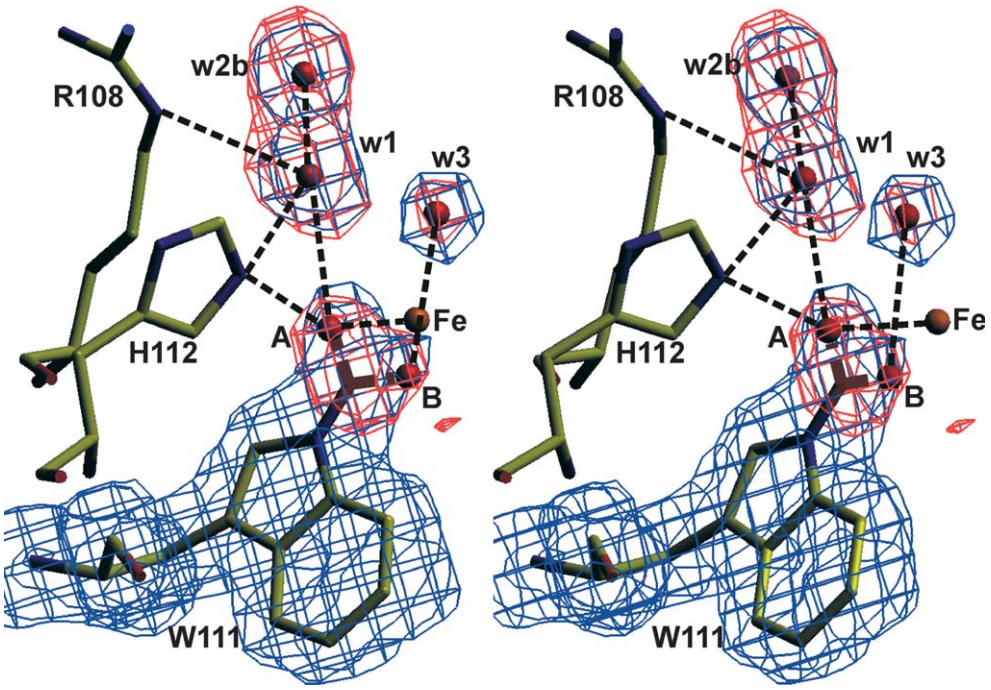

Figure 4. Stereo view of the distal side heme cavity. The $2F_o-F_c$ (blue) electron density map of Trp111 with its putative perhydroxy modification and three water molecules is modeled at $\sigma=1.0$. The two possible locations of the OH of the perhydroxy group are indicated by A and B, and are joined to the N–O with broken lines. The maps were calculated assuming equal occupancy of the two locations. The F_o-F_c (red) electron density map (modeled at $\sigma=3.0$) calculated without the perhydroxy group or the three water molecules in the model is superimposed. Potential hydrogen bonds are indicated by broken lines in black. Water molecules, w1 and w2b, are the same as those thatappear in Figure 3 with the same labels. The Figure was prepared using SETOR.[24]

(Figure 4). Speculation on the origin and role of the modification may be premature in the absence of independent corroborating evidence. However, Trp111 is required for the reduction of compound I and the putative modification hints at a role involving more than simple hydrogen bonding of H_2O_2. Furthermore, postulating an inductive effect of the Met-Tyr adduct attached to Trp111 as being required for addition of the perhydroxy modification to the Trp provides an explanation for the essential role of the adduct in the catalase reaction.

The unassigned electron density in the main channels leading to the heme cavities in both subunits of the native enzyme[16] (Figure 3(a)) is visible also in the maps of the variant (Figure 3(b)) and is accompanied by additional nearby regions of unassigned density, particularly in subunit B (data not shown), which is suggestive of a relatively large, but partially disordered, molecule. The portion of the molecule with strongest density, first observed in the native maps (Figure 3(a)), is nestled in a cavity on the side of the channel almost completely surrounded by a mixture of non-polar (Pro140 C^{α}–C^{β}, Ala143 methyl, Ala290 methyl and Val293 isopropyl) and polar (Thr323 carbonyl, Trp309 indole N, Pro140 carbonyl and Ser324 carbonyl) surfaces. The presence of the same apparent molecule in Ser324Thr, which has a lower affinity for INH, suggests something other than the INH-like pyridine derivative originally speculated,[16] and the high affinity of KatG for NADH provides a possible candidate. Identification of the molecule will undoubtedly provide insight into the *in vivo* substrate(s) of KatG.

The peroxidase substrates, ABTS and *o*-dianisidine, are significantly larger than INH, making it unlikely that they bind in the same cavity as is occupied by INH,[19] benzyhydroxamic acid[21] and salicylhydroxamic acid[22] in plant peroxidases, a surmise supported by the unchanged peroxidase specific activity of the Ser324Thr variant. Like the identity of the peroxidase substrate of KatG, the site of its binding remains to be determined, and a more distant binding site, as in cytochrome *c* peroxidase and lignin peroxidase, remains a possibility.

Protein Data Bank accession number

Structure factors and coordinates have been submitted to the Protein Data Bank under the accession number 1X7U.

Acknowledgements

This work was supported by grant OGP9600 from the Natural Sciences and Engineering Research Council of Canada (to P.C.L.), by the Canadian Research Chair Program (to P.C.L.) and by

fellowship EX-2003-0866 from the Ministerio de Educación Cultura y Deporte, Spain (to X.C.).

References

1. Nicholls, P., Fita, I. & Loewen, P. C. (2001). Enzymology and structure of catalases. *Advan. Inorg. Chem.* **51**, 51–106.
2. Singh, R., Wiseman, B., Deemagarn, T., Donald, L., Duckworth, H. E., Carpena, X., Fita, I. & Loewen, P. C. (2004). Catalase-peroxidases (KatG) exhibit NADH oxidase activity. *J. Biol. Chem.* **279**, 43098–43106.
3. Zhang, Y., Heym, B., Allen, B., Young, D. & Cole, S. (1992). The catalase-peroxidase gene and isoniazid resistance of *Mycobacterium tuberculosis*. *Nature*, **358**, 591–593.
4. Rozwarski, D. A., Grant, G. A., Barton, D. H. R., Jacobs, W. R. & Sacchettini, J. C. (1998). Modification of the NADH of the isoniazid target (InhA) from *Mycobacterium tuberculosis*. *Science*, **279**, 98–102.
5. Lei, B., Wei, C. J. & Tu, S. C. (2000). Action mechanism of antitubercular isoniazid: activation by *Mycobacterium tuberculosis* KatG, isolation and characterization of InhA inhibitor. *J. Biol. Chem.* **275**, 2520–2526.
6. Wilming, M. & Johnsson, K. (1999). Spontaneous formation of the bioactive form of the tuberculosis drug isoniazid. *Angew. Chem. Int. Ed.* **38**, 2588–2590.
7. Mdluli, K., Slayden, R. A., Zhu, Y., Ramaswamy, S., Pan, X., Mead, D. *et al*. (1998). Inhibition of a *Mycobacterium tuberculosis* β-ketoacyl ACP synthase by isoniazid. *Science*, **280**, 1607–1610.
8. Heym, B., Alzari, P. M., Honoré, N. & Cole, S. T. (1995). Missense mutations in the catalase-peroxidase gene, katG are associated with isoniazid resistance in *Mycobacterium tuberculosis*. *Mol. Microbiol.* **15**, 235–245.
9. Johnsson, K. & Schultz, P. G. (1994). Mechanistic studies of the oxidation of isoniazid by the catalase-peroxidase from *Mycobacterium tuberculosis*. *J. Am. Chem. Soc.* **116**, 7425–7426.
10. Johnsson, K., King, D. S. & Schultz, P. G. (1995). Studies on the mechanism of action of isoniazid and ethionamide in the chemotherapy of tuberculosis. *J. Am. Chem. Soc.* **117**, 5009–5010.
11. Wang, J. Y., Burger, R. M. & Drlica, K. (1998). Role of superoxide in catalase-peroxidase mediated isoniazid action against Mycobacteria. *Antimicrob. Agents Chemother.* **42**, 709–711.
12. Wei, C. J., Lei, B., Musser, J. M. & Tu, S. C. (2003). Isoniazid activation defects in recombinant *Mycobacterium tuberculosis* catalase-peroxidase (KatG) mutants evident in InhA inhibitor production. *Antimicrob. Agents Chemother.* **47**, 670–675.
13. Yamada, Y., Saijo, S., Sato, T., Igarashi, N., Usui, H., Fujiwara, T. & Tanaka, N. (2001). Crystallization and preliminary X-ray analysis of catalase-peroxidase from the halophilic archaeon *Haloarcula marismortui*. *Acta Crystallog. sect. D*, **57**, 1157–1158.
14. Yamada, Y., Fujiwara, T., Sato, T., Igarashi, N. & Tanaka, N. (2002). The 2.0 Å crystal structure of catalase-peroxidase from *Haloarcula marismortui*. *Nature Struct. Biol.* **9**, 691–695.
15. Carpena, X., Switala, J., Loprasert, S., Mongkolsuk, S., Fita, I. & Loewen, P. C. (2002). Crystallization and preliminary X-ray analysis of the catalase-peroxidase KatG from *Burkholderia pseudomallei*. *Acta Crystallog. sect. D*, **58**, 2184–2186.
16. Carpena, X., Loprasert, S., Mongkolsuk, S., Switala, J., Loewen, P. C. & Fita, I. (2003). Catalase-peroxidase KatG of *Burkholderia pseudomallei* at 1.7 Å resolution. *J. Mol. Biol.* **327**, 475–489.
17. Wada, K., Tada, T., Nakamura, Y., Kinoshita, T., Tamoi, M., Sigeoka, S. & Nishimura, K. (2002). Crystallization and preliminary X-ray diffraction studies of catalase-peroxidase from *Synechococcus* PCC7492. *Acta Crystallog. sect. D*, **58**, 157–159.
18. Bertrand, T., Eady, N. A. J., Jones, J. N., Nagy, J. M., Jamart-Grégoire, B., Raven, E. L. & Brown, K. A. (2004). Crystal structure of *Mycobacterium tuberculosis* catalase-peroxidase. *J. Biol. Chem.* **279**, 39000–39009.
19. Pierattelli, R., Banci, L., Eady, N. A. J., Bodiquel, J., Jones, J. N., Moody, P. C. E. *et al*. (2004). Enzyme-catalyzed mechanism of isoniazid activation in class I and class III peroxidases. *J. Biol. Chem.* **279**, 38991–38999.
20. Yu, S., Girotto, S., Zhao, X. & Magliozzo, R. S. (2003). Reduced affinity for isoniazid in the S315T mutant of *Mycobacterium tuberculosis* KatG is a key factor in antibiotic resistance. *J. Biol. Chem.* **278**, 44121–44127.
21. Henriksen, A., Schuller, D. J., Meno, K., Welinder, K. G., Smith, A. T. & Gajhede, M. (1998). Structural interactions between horseradish peroxidase C and the substrate benzhydroxamic acid determined by X-ray crystallography. *Biochemistry*, **37**, 8054–8060.
22. Sharp, K. H., Moody, P. C. E., Brown, K. A. & Raven, E. L. (2004). Crystal structure of the ascorbate peroxidase–salicylhydroxamic acid complex. *Biochemistry*, **43**, 8644–8651.
23. Rawat, R., Whitty, A. & Tonge, P. J. (2003). The isoniazid-NAD adduct is slow, tight binding inhibitor of InhA, the *Mycobacterium tuberculosis* enoyl reductase: adduct affinity and drug resistance. *Proc. Natl Acad. Sci. USA*, **100**, 13881–13886.
24. Evans, S. (1993). SETOR: hardware lighted three-dimensional solid model representations of macromolecules. *J. Mol. Graph.* **11**, 134–138.
25. Kleywegt, G. J. & Jones, T. A. (1994). Detection, delineation, measurement and display of cavities in macromolecule structures. *Acta Crystallog. sect. D*, **50**, 178–185.
26. Maté, M. J., Sevinc, M. S., Hu, B., Bujons, J., Bravo, J., Switala, J. *et al*. (1999). Mutants that later the covalent structure of catalase hydroperoxidase II from *Escherichia coli*. *J. Biol. Chem.* **274**, 27717–27725.
27. Rorth, H. M. & Jensen, P. K. (1967). Determination of catalase activity by means of the Clark electrode. *Biochim. Biophys. Acta*, **139**, 171–173.
28. Auclair, C. & Voisin, E. (1985). Nitroblue tetrazolium reduction. In *CRC Handbook of Methods for Oxygen Radical Research* (Greenwald, R. A., ed.), pp. 123–132, CRC Press, Boca Raton, FL.
29. Layne, E. (1957). Spectrophotometric and turbidimetric methods for measuring proteins. *Methods Enzymol.* **3**, 447–454.
30. Donald, L. J., Krokhin, O. V., Duckworth, H. W., Wiseman, B., Deemagarn, T., Singh, R. *et al*. (2003). Characterization of the catalase-peroxidase KatG from *Burkholderia pseudomallei* by mass spectrometry. *J. Biol. Chem.* **278**, 35687–35692.
31. Otwinowski, Z. & Minor, W. (1996). Processing of X-ray diffraction data collected in oscillation mode. *Methods Enzymol.* **276**, 307–326.
32. Navaza, J. (1994). AMoRe: an automated package for molecular replacement. *Acta Crystallog. sect. A*, **50**, 157–163.
33. Murshudov, G. N., Vagin, A. A. & Dodson, E. J. (1997).

Refinement of macromolecular structures by the maximum-likelihood method. *Acta Crystallog. sect. D*, **53**, 240–255.
34. Collaborative Computational Project, Number 4. (1994). The CCP4 suite: programs for protein crystallography. *Acta Crystallog. sect. A*, **50**, 760–763.
35. Jones, T. A., Zou, J. Y., Cowan, S. W. & Kjeldgaard, M. (1991). Improved methods for building protein models in electron density maps. *Acta Crystallog. sect. A*, **47**, 110–119.

Edited by R. Huber

(Received 17 August 2004; received in revised form 27 September 2004; accepted 11 October 2004)